Antiferromagnetic-ferromagnetic phase transition in FeRh probed by x-ray magnetic circular dichroism

C. Stamm,[1,*] J.-U. Thiele,[2] T. Kachel,[1] I. Radu,[1,3] P. Ramm,[3] M. Kosuth,[4] J. Minár,[4] H. Ebert,[4] H. A. Dürr,[1] W. Eberhardt,[1] and C. H. Back[3]

[1]*BESSY GmbH, Albert-Einstein-Strasse 15, 12489 Berlin, Germany*

[2]*Hitachi Global Storage Technologies, San Jose Research Center, 3403 Yerba Buena Road, San Jose, California 95135, USA*

[3]*Department of Physics, Universität Regensburg, 93040 Regensburg, Germany*

[4]*Department of Chemistry and Biochemistry, Ludwig-Maximilians University, 81377 Munich, Germany*

(Received 10 January 2008; revised manuscript received 2 April 2008; published 2 May 2008)

The phase transition from antiferromagnetic to ferromagnetic ordering in FeRh is investigated in an element specific way by means of x-ray absorption spectroscopy. Dichroism sum rules allow us to determine spin and orbital moments of the two elements as the system is driven through the phase transition. Increasing the temperature from 300 to 450 K, the magnetic moments in Fe and Rh both evolve from zero to their final value, while the ratio of Rh to Fe moments stays constant. Our experimental findings are supported by the results of fully relativistic *ab initio* calculations.

DOI: 10.1103/PhysRevB.77.184401 PACS number(s): 75.50.Bb, 75.70.−i, 78.70.Dm

It has been known for about 70 years that the chemically ordered phase of the alloy FeRh near the equiatomic composition undergoes a phase transition from an antiferromagnetic (AFM) to a ferromagnetic (FM) phase at around $T_p = 370$ K.[1,2] At room temperature, the CsCl-type structured alloy has zero net magnetic moment; the Fe spins antiferromagnetically order with $\pm 3.3\mu_B$, while the Rh spins do not exhibit any ordering.[3,4] Upon heating beyond a critical temperature T_p, FeRh undergoes an isotropic lattice expansion and the Fe as well as the Rh spins align ferromagnetically. Magnetic moments of $3.04\mu_B$ for Fe and $0.62\mu_B$ for Rh were reported[3] on a sample with 53 at. % Rh. When the temperature is raised above the Curie temperature, which is typically found to be around $T_c = 740$ K,[5,6] the system undergoes a second phase transition into the paramagnetic phase. Both temperatures T_c and T_p are sensitive to the exact composition of the sample and may be tuned by doping. For bulk samples of $Fe_{48}Rh_{52}$, the AFM-FM phase transition occurs close to room temperature, but by doping with Pt or Ir it can be adjusted to above 500 K.[5,7] It has been discussed that this opens up some interesting possibilities for technological applications, in particular, for heat assisted magnetic recording. Consequently, in recent experiments, this phase transition was studied as a function of the time elapsed after excitation with a strong optical pulse.[8–11] It has been shown that ultrafast heating of the FeRh system via laser pulse excitation seems to trigger the phase transition on picosecond time scales. However, in stroboscopic laser pump-probe experiments, only the repetitive part of the phase transition can be probed, which requires that the transition has to be studied in rather large magnetic fields to guarantee repeatability. Thus, it is evident that for a deeper understanding of the fast magnetic response observed in recent experiments, a thorough investigation of the static properties on macroscopic and microscopic length scales is required.

In this paper, we investigate the AFM to FM phase transition by using x-ray absorption spectroscopy (XAS), in particular, x-ray magnetic circular dichroism (XMCD). The measurements were taken in a transmission setup at beamline UE 56/1 at BESSY, by using circularly polarized soft x rays. XMCD sum rules[12,13] allow us to monitor the evolution of spin and orbital magnetic moments while going through the phase transition. Whereas previously the absorption of hard x rays at the Rh $L_{2,3}$ edges around 3 keV was measured,[14] in our experiment we explore the Fe $L_{2,3}$ and Rh $M_{2,3}$ absorption edges, thus simultaneously measuring both constituents at the same spectrometer. A sum rule analysis yields the spin and orbital magnetic moments of both elements in the ordered alloy as a function of temperature around the phase transition. We propose a microscopic model describing the intermediate state as an inhomogeneous mixture of the AFM and FM phases. The experimental results obtained by XMCD are compared to *ab initio* band structure calculations and good agreement is found for the Fe and Rh absorption spectra as well as the dichroic signal.

The FeRh samples were grown by magnetron sputtering from an $Fe_{47}Rh_{53}$ alloy target. By adjusting the pressure of the Ar gas, a composition of $Fe_{48.5}Rh_{51.5}$ was obtained in the films as confirmed by Rutherford backscattering. We slightly increased the transition temperature by doping the films with 1%–2% of Ir by cosputtering from an Ir element target. The FeRh films were grown on 50 nm thick Si_3N_4 membranes of 2×2 mm^2 size. A 2 nm thick Pt buffer layer was used, which results in (111) textured growth of the FeRh. More information on the sample growth can be found in Refs. 5 and 15. To be able to measure a reasonable x-ray intensity in transmission, we have used a rather thin FeRh film of 25 nm thickness. On top, a 200 nm thick Cu heat sink was deposited as this sample had also been used for time resolved XMCD studies.[11] The film was capped by a 2 nm thick Pt layer to prevent oxidation. The sample cross section is sketched in Fig. 1(b).

Prior to the XMCD experiments, the sample was characterized by using a temperature-dependent vibrating sample magnetometry (VSM) setup. The resulting temperature hysteresis curve is depicted in Fig. 1(a). The transition temperatures (here defined as the mean value between the onset and end of the slope ± half the transition temperature interval)

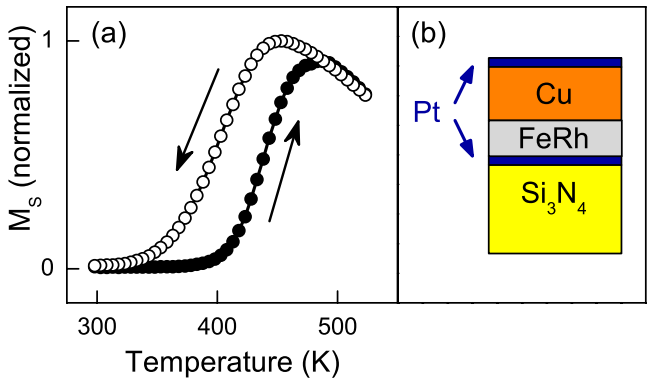

FIG. 1. (Color online) VSM measurement of the saturated magnetic moment as a function of temperature is shown in (a). ● and ○ denote measurements while increasing (decreasing) the temperature, respectively (see the arrows). The sample cross section is sketched in (b).

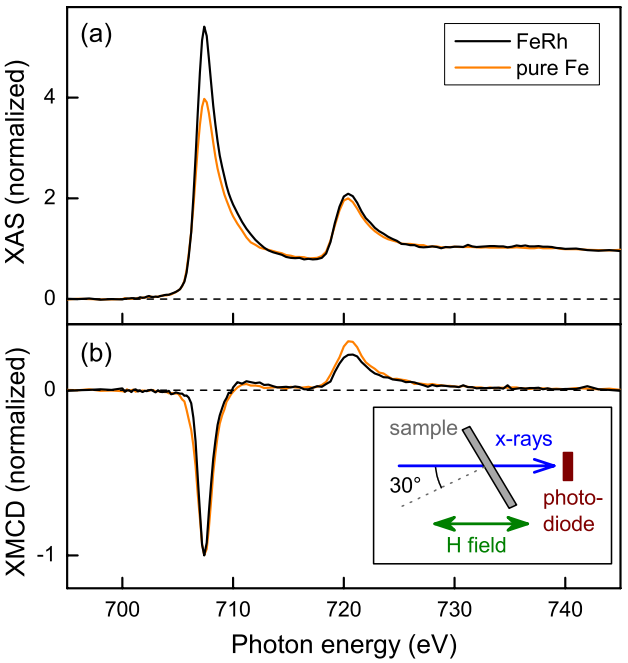

FIG. 2. (Color online) Comparison of measured XAS (a) and XMCD (b) of FeRh (black line, $T=420$ K) and pure Fe (bright red line, $T=300$ K). The absorption spectra in (a) are normalized to an edge jump equal to 1. The dichroism in (b) is normalized to −1 at the Fe L_3 peak. The geometry of the transmission measurement is drawn in the inset.

can be estimated to be 440 ± 50 and 385 ± 60 K upon heating and cooling, respectively. The transitions in the heating and cooling cycle are significantly broader than observed in the single crystal and highly textured polycrystalline films grown under similar conditions used in previous studies.[6,9,15] This is presumably due to the SiN substrate and the choice of a rather thin Pt seed layer, which result in a somewhat lower degree of texture compared to that of other samples.

To support the interpretation of our experimental results, we performed first-principles calculations on the basis of local-spin-density approximation (LSDA)[16] to density functional theory. For this purpose, we employed the spin-polarized relativistic Korringa–Kohn–Rostoker Green's function (SPR-KKR) method.[17] As a first step of our investigation, we performed self-consistent calculations for bulk FeRh using the CsCl structure with the experimental lattice constant of 3.09 Å. For the calculations of the corresponding XAS and XMCD spectra, we used an expression based on Fermi's golden rule that was implemented within the SPR-KKR method.[18] For a direct comparison of the calculated absorption coefficient to experimental data, the corresponding theoretical spectra were broadened in the conventional way.[18] This means, in particular, that Lorentzian broadening (0.3 eV) was applied to account for the lifetime of the core hole and excited electrons. In addition, Gaussian broadening (0.4 eV) was used to represent finite experimental resolution.

In Fig. 2, we show measured XAS and XMCD spectra of the FeRh film in the FM phase and compare them to the spectra of a pure Fe film. Circularly polarized x rays were transmitted through the films, which were tilted by an angle of 30° away from perpendicular incidence (see the inset of Fig. 2). An alternating magnetic field of ± 0.5 T was applied along the x-ray beam direction at each photon energy. This resulted in two spectra with opposite orientations of the applied field that are almost simultaneously recorded, i.e., without any significant change in incident x-ray intensity. The XAS spectrum is obtained by averaging the absorption for both field orientations, whereas XMCD is calculated as their difference. The absorption was calculated by normalizing the transmitted with the incoming x-ray intensity (total electron yield of the last Au-coated mirror), correcting for the energy-dependent sensitivity of the photodiode detector, and applying the natural logarithm. A comparison of the FeRh film to the 15 nm Fe film reveals that while the XAS peak positions are unchanged, the absorption around the L_3 resonance is enhanced in FeRh with respect to the pure Fe film. This increase in the branching ratio is evidence for an increased LS coupling in FeRh.[19] The XMCD spectrum in Fig. 2(b) exhibits a decreased relative dichroic signal at the L_2 edge, which reflects a stronger orbital moment contribution m_L/m_S in the FeRh film. The same trend is also found in the theoretical data. However, the experimental data show a more pronounced reduction. This may be due to the known underestimation of Fe orbital moment calculated within LSDA.[20] The theoretical values found for m_L/m_S are 0.023 for Fe and 0.059 for Rh. When comparing the measured XAS and XMCD spectra to *ab initio* band structure calculations in Fig. 3, quite good agreement is found for the Fe and Rh absorption. Notice that the experimental XMCD is smaller by roughly a factor of 2. We will discuss this later when evaluating the magnetic moments as a function of sample temperature. The additional small peak in the Rh spectrum at 519.4 eV is attributed to absorption in the Pt buffer layers.

The temperature-dependent behavior around the AFM to FM phase transition can now be investigated by measuring hysteresis loops at different temperatures, as shown in Fig. 4. The transmitted intensities at the Fe L_3 and Rh M_3 edges were recorded while ramping the applied field, which reveals the growth in saturation magnetization upon ferromagnetic ordering. The signal from the Rh edge, although much weaker, exhibits the same magnetization loop as the Fe edge.

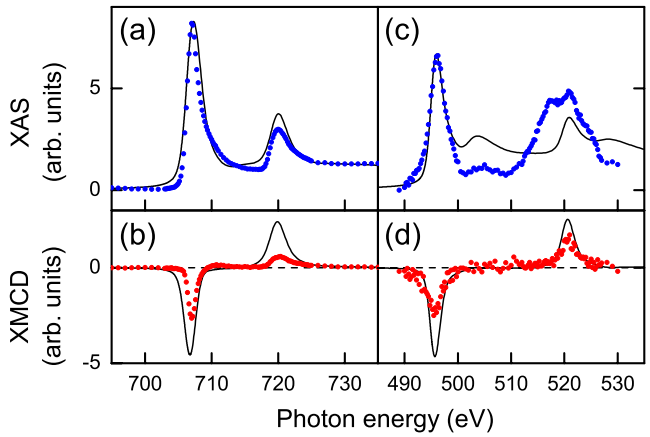

FIG. 3. (Color online) Calculated XAS and XMCD spectra (lines) of FeRh are compared to the measured ones (dots). In (a) and (c), the isotropic spectra $(I_+ + I_-)/2$ are drawn for the Fe and Rh absorption edges, respectively. Dichroism $(I_+ - I_-)$ at the Fe edge is plotted in (b) and the Rh edge in (d).

The film is completely switched above a field of 0.2 T; however, the magnetization still increases as it is pulled out of the plane toward the direction of the applied field.

XMCD measurements across the Fe and Rh absorption edges are displayed in Fig. 5. During the measurement, the temperature was increased stepwise from 300 to 450 K. At each temperature, dichroic spectra at the Fe and Rh edges were measured, as well as hysteresis loops (see Fig. 4). We observe a monotonous increase in the Fe and Rh dichroic signals with increasing temperature and explore this in a quantitative way in the following sum rule analysis.

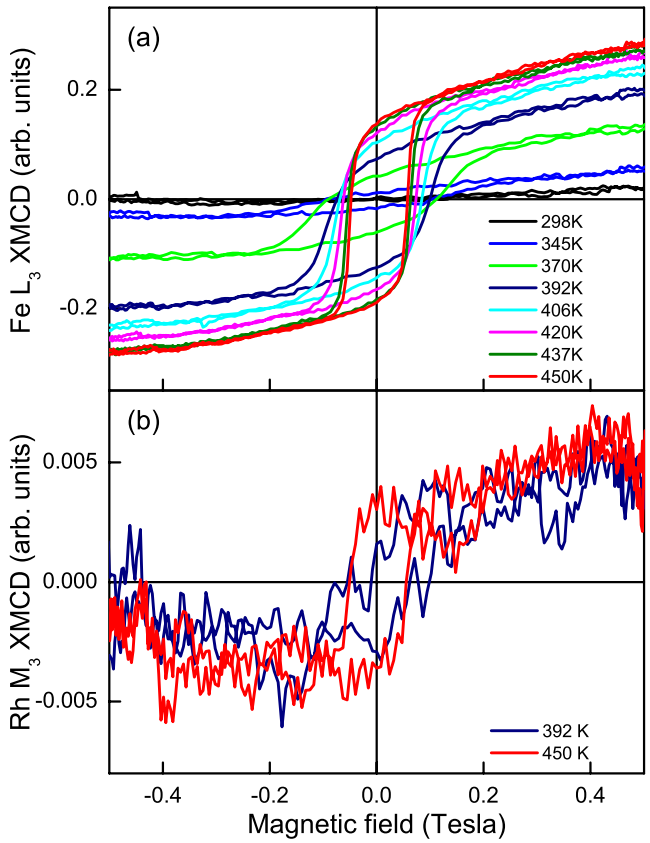

FIG. 4. (Color online) Magnetic hysteresis loops of the Fe and Rh components, measured at the Fe L_3 and Rh M_3 edges, are plotted in (a) and (b), respectively. The transmitted x-ray intensity was measured as a function of the applied field, normalized by the incident flux, and the resulting curves were centered on zero by subtracting the mean intensity.

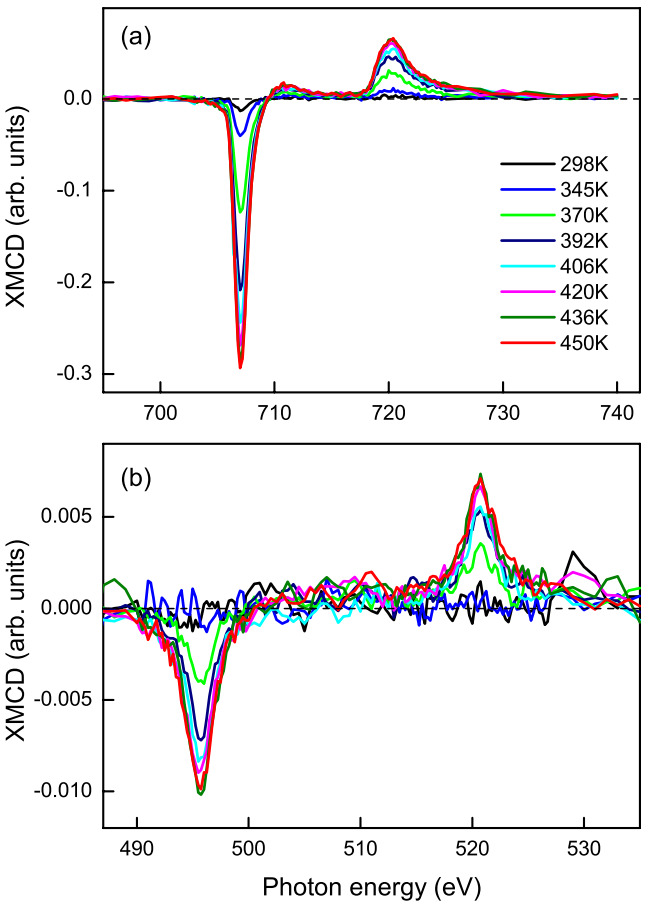

FIG. 5. (Color online) XMCD of the FeRh film at fixed temperatures between 300 and 450 K. Measured data at the Fe L and Rh M absorption edges are displayed in (a) and (b), respectively. A magnetic field of ± 0.5 T was applied along the x-ray propagation direction, which enclosed an angle of 30° with the sample surface normal. Due to the low absorption cross section of the Rh M edges, two consecutive Rh spectra were averaged.

Integrating XMCD over the $L_{2,3}$ edges of Fe and $M_{2,3}$ edges of Rh, respectively, allows us to determine the spin and orbital moments of the two elements.[12,13,21] Figure 6(a) summarizes the resulting magnetic moments as a function of sample temperature. First XMCD measurements on FeRh by Chaboy *et al.*[14] determined the Rh magnetic moments by absorption of hard x rays at the Rh $L_{2,3}$ edges. Chaboy *et al.*[14] found that the AFM to FM transition is replaced by a transition between two different FM phases: a maximum moment of $m_{\mathrm{Rh}} \approx 1 \mu_B$ at 180 K and a reduced moment of $\approx 0.7 \mu_B$ at lower temperatures. In contrast, we do not observe significant magnetic moments at low temperatures. The curve rather demonstrates the expected AFM to FM phase transition[1,2] with a slightly enhanced transition temperature due to Ir doping.[5,7] It is apparent that the XMCD

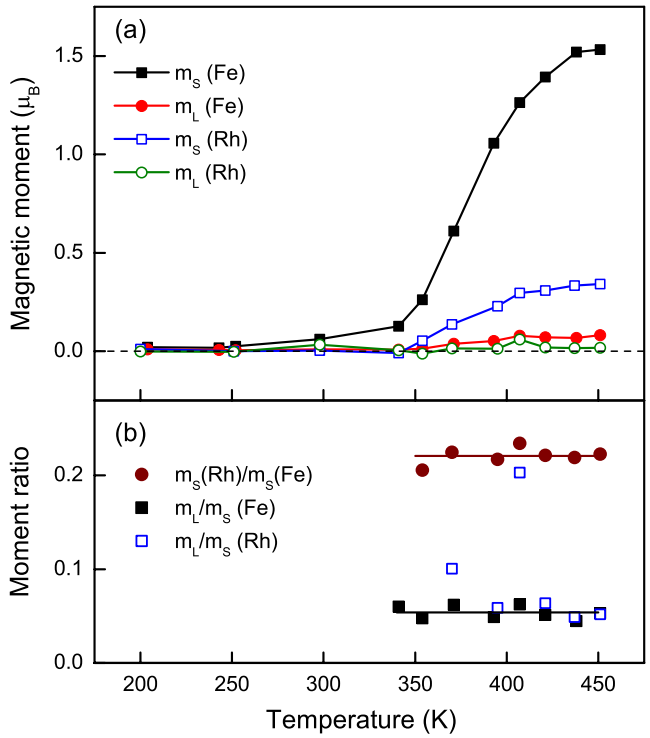

FIG. 6. (Color online) XMCD sum rule analysis of the FeRh spectra in Fig. 5. In (a), the spin (m_S, squares) and orbital (m_L, circles) magnetic moments of Fe (filled symbols) and Rh (open symbols) are plotted as a function of temperature. In (b), the ratio of the Rh to Fe spin moments is plotted as circles and the orbital to spin moment ratio for Fe (Rh) is plotted as filled (open) squares, respectively. The lines reflect their average value.

results exhibit a somewhat lower transition temperature $T_p = 375 \pm 75$ K upon heating than the VSM measurement in Fig. 1. The biggest difference, beyond the mere duration of the measurement, is given by the sample design. To allow for x-ray transmission, a Si wafer supporting a Si_3N_4 membrane of 2×2 mm^2 size is used as a substrate for the FeRh film. In VSM, the magnetic moment of the FeRh film is summed over the whole wafer (5×10 mm^2), with the area of the membrane contributing only 8% to the signal. It is known that the substrate can change the value of T_p.[15]

Several assumptions have to be made in order to get quantitative numbers from the sum rule analysis. First, the size of the magnetic moments is proportional to the number of empty states in the topmost d shell, i.e., holes $n_h = (10 - n_d)$. Calculated electron occupation numbers of $n_{3d}(\mathrm{Fe}) = 6.49$ and $n_{4d}(\mathrm{Rh}) = 7.66$ were used. Second, special care has to be taken to account for absorption into delocalized states, both in the film and the substrate. A two-step function with amplitude of 2/3 at the $p_{3/2}$ edge and 1/3 at the $p_{1/2}$ edge was used to remove the edge jump in the absorption spectrum.[21] Furthermore, in our analysis, we neglected the magnetic dipolar term, which generally has a contribution to the spin moment. It was found by the calculations that this term is on the order of $10^{-4}\mu_B$ and is comparable to values for other polycrystalline samples.[22,23] Note that the experimentally determined moments are somewhat smaller than the ones calculated by *ab initio* theory, which amount to $3.15\mu_B$ for the spin moment of Fe, $0.072\mu_B$ for the orbital moment of Fe, $0.96\mu_B$ for the spin moment of Rh, and $0.057\mu_B$ for the orbital moment of Rh. Two reasons are responsible for the reduction in the measured moments. First, the calculations are performed at 0 K. The experimental moments are thus reduced by about 20%.[2] Second, the applied field encloses an angle of 60° with the in-plane easy axis; see the inset of Fig. 2. The equilibrium direction of the magnetization is determined by minimizing the sum of Zeeman and dipolar energy. However, XMCD measures the component of the magnetic moment parallel to the x-ray propagation direction. This leads to a further reduction in the measured moments by 25%, as was determined by calculating the corresponding hysteresis loop. When correcting for the latter factor, our measurement results in $2.2\mu_B$ for the total Fe moment and $0.5\mu_B$ for the total Rh moment, as measured at an elevated temperature of 450 K. This is in quite good agreement with VSM measurements on similar films,[5] where a net magnetization of ≈ 1000 emu/cm^3 was found, which corresponds to $\approx 2.9\mu_B$ per unit cell consisting of one Fe and one Rh atom. As our sample has a higher AFM to FM transition temperature due to Ir doping, the maximum magnetic moments are reduced compared to those of pure FeRh samples.[7]

We can now plot various ratios of the evaluated moments in Fig. 6(b). As soon as the moments are well defined after the onset of the transition, all ratios can be described very well by a constant. One finds that the Rh spin is about 22% of the Fe spin. The constant ratio means that they both exhibit the same increase with increasing temperature. As usually found in solids, the orbital moments in FeRh are strongly quenched. The iron orbital moment reflects the same increase with temperature as its spin counterpart. A ratio of $m_L/m_S = 0.054$ is found for the Fe contribution in FeRh. This is a 20% increase of the value found in pure Fe, being 0.044 (from Ref. 21, also found when evaluating the data in Fig. 2). The Rh orbital moments are rather small and, thus, their error bars are considerably larger. However, a similar ratio m_L/m_S is found at the Rh sites.

Notice that the ratios in Fig. 6(b) can all be described by a constant while the individual moments still increase with rising temperature. This suggests the following microscopic scenario for the buildup of the FM order. Starting from the AFM phase and increasing the temperature, microscopic parts of the film start to ferromagnetically order, as was found in temperature-dependent domain mapping by means of magnetic force microscopy (MFM).[24,25] Our x-ray beam that is transmitted through the sample has a finite size of about 100×500 μm^2, averaging the FM domains over an area of that size and over the thickness of the film. Even if the measured moments are still quite small during an early stage of the AFM to FM transition, the moment ratios already reflect the same value as for the fully FM ordered phase. This means that the early stage microscopic FM domains are in the same state as the fully FM phase. Our results thus suggest that both AFM and FM phases coexist within the temperature interval of 300–450 K and that their relative size changes according to the temperature. This scenario is confirmed by temperature-dependent neutron scattering, wherein a gradual decrease in the AFM scattering peak

coincides with the increase in the saturation magnetization.[6] The existence of local magnetic moments in FeRh was postulated before to explain the dynamic processes when driving the phase transition by an ultrafast laser pulse.[10] Here, we argue that this also holds for the film in thermal equilibrium, a scenario that is further supported by temperature-dependent MFM studies[24,25] and neutron scattering combined with magnetic measurements.[6]

To summarize, we have investigated the phase transition of a 25 nm thin FeRh film, from antiferromagnetic order at room temperature to ferromagnetic order at 450 K. Applying XMCD sum rules, spin and orbital magnetic moments are evaluated. We find that while the moments increase during the rather wide transition region, at the same time the relative moments stay constant. This can be attributed to an inhomogeneous state, in which domains of ferromagnetic order coexist with areas that are still antiferromagnetic.

Financial support by the Deutsche Forschungsgemeinschaft through the Priority Programme 1133 "Ultra Fast Magnetization Processes" and 689 "Spin phenomena in reduced dimensions" is acknowledged.

*christian.stamm@bessy.de

[1] M. Fallot and R. Horcart, Rev. Sci. **77**, 498 (1939).
[2] J. S. Kouvel and C. C. Hartelius, J. Appl. Phys. **33**, 1343 (1962).
[3] E. F. Bertaut, A. Delapalme, F. Forrat, G. Roult, F. de Bergevin, and R. Pauthenet, J. Appl. Phys. **33**, 1123 (1962).
[4] V. L. Moruzzi and P. M. Marcus, Phys. Rev. B **46**, 2864 (1992).
[5] J.-U. Thiele, S. Maat, and E. E. Fullerton, Appl. Phys. Lett. **82**, 2859 (2003).
[6] J.-U. Thiele, S. Maat, J. L. Robertson, and E. E. Fullerton, IEEE Trans. Magn. **40**, 2537 (2004).
[7] J. S. Kouvel, J. Appl. Phys. **37**, 1257 (1966).
[8] G. Ju, J. Hohlfeld, B. Bergman, R. J. M. van de Veerdonk, O. N. Mryasov, J.-Y. Kim, X. Wu, D. Weller, and B. Koopmans, Phys. Rev. Lett. **93**, 197403 (2004).
[9] J.-U. Thiele, M. Buess, and C. H. Back, Appl. Phys. Lett. **85**, 2857 (2004).
[10] B. Bergman, G. Ju, J. Hohlfeld, R. J. M. van de Veerdonk, J.-Y. Kim, X. Wu, D. Weller, and B. Koopmans, Phys. Rev. B **73**, 060407(R) (2006).
[11] I. Radu, C. Stamm, T. Kachel, N. Pontius, P. Ramm, J.-U. Thiele, H. A. Dürr, W. Eberhardt, and C. H. Back (unpublished).
[12] B. T. Thole, P. Carra, F. Sette, and G. van der Laan, Phys. Rev. Lett. **68**, 1943 (1992).
[13] P. Carra, B. T. Thole, M. Altarelli, and X. Wang, Phys. Rev. Lett. **70**, 694 (1993).
[14] J. Chaboy, F. Bartolome, M. R. Ibarra, C. I. Marquina, P. A. Algarabel, A. Rogalev, and C. Neumman, Phys. Rev. B **59**, 3306 (1999).
[15] S. Maat, J. U. Thiele, and E. E. Fullerton, Phys. Rev. B **72**, 214432 (2005).
[16] S. H. Vosko, L. Wilk, and M. Nusair, Can. J. Phys. **58**, 1200 (1980).
[17] H. Ebert, in *Electronic Structure and Physical Properties of Solids*, Lecture Notes in Physics Vol. 535, edited by H. Dreyssé (Springer, Berlin, 2000), p. 191.
[18] J. Minárt and H. Ebert, Appl. Phys. A: Mater. Sci. Process. **78**, 847 (2004).
[19] B. T. Thole and G. van der Laan, Phys. Rev. B **38**, 3158 (1988).
[20] Induced moments such as of Rh are generally calculated more accurately within LSDA.
[21] C. T. Chen, Y. U. Idzerda, H.-J. Lin, N. V. Smith, G. Meigs, E. Chaban, G. H. Ho, E. Pellegrin, and F. Sette, Phys. Rev. Lett. **75**, 152 (1995).
[22] J. Stöhr and H. König, Phys. Rev. Lett. **75**, 3748 (1995).
[23] H. A. Dürr and G. van der Laan, Phys. Rev. B **54**, R760 (1996).
[24] Y. Yokoyama, M. Usukura, S. Yuasa, Y. Suzuki, H. Miyajima, and T. Katayama, J. Magn. Magn. Mater. **177-181**, 181 (1998).
[25] M. Manekar, C. Mukherjee, and S. B. Roy, EPL **80**, 17004 (2007).